http://dx.doi.org/10.5012/bkcs.2013.34.12.3586

ZnO on Thiolated Graphene Oxide as Efficient Photocatalyst for Degradation of Methylene Blue

Yu Hyun Kim and Hyun Chul Choi*

Department of Chemistry and Institute of Basic Science, Chonnam National University, Gwangju 500-757, Korea
**E-mail: chc12@chonnam.ac.kr*
Received August 13, 2013, Accepted September 9, 2013

We present here an efficient and simple method for preparation of highly active heterogeneous ZnO photocatalyst (graphene oxide-zinc oxide: GO-ZnO), specifically by deposition of ZnO nanoparticles onto thiolated GOs. The resultant GO-ZnO sample was characterized by TEM, XRD, Auger, XPS, and Raman measurements, revealing that the size-similar and quasi-spherical ZnO nanoparticles were anchored to the thiolated GO surfaces. The average particle diameter was about 2.5 nm. In the photodegradation of methylene blue (MB) under ultraviolet (UV) light, GO-ZnO exhibited remarkably enhanced photocatalytic efficiency compared with thiolated GO and pure ZnO particles. This strong photocatalytic performance of GO-ZnO can be attributed to the suppression of electron recombination and the enhancement of mass transportation. The results showed that thiolated GO is the preferable supporting material.

Key Words : Thiolated graphene oxide, GO-ZnO, Photocatalyst, Methylene blue

Introduction

Semiconductor-assisted photocatalysis has recently emerged as an efficient method for conversion of photon energy into chemical energy and environmental purification.[1,2] Among the semiconducting catalysts, zinc oxide (ZnO) has been extensively studied due to its low cost, non-toxicity, outstanding stability, and high efficiency.[3-5] When ZnO particles are illuminated with ultraviolet (UV) light, electron/hole pairs are generated. These electrons and holes can migrate and initiate redox reactions with water and oxygen, by which they degrade organic molecules absorbed on the surface of a photocatalyst.[6,7] Nano-sized ZnO particles, owing to their large surface area, can be effectively utilized to enhance photocatalytic activity.[8-11] Unfortunately, in nano-sized particles, agglomeration occurs more readily; the resultant difficulty of their separation and recycling from the reaction system after photocatalysis hinders their application in this field. Thus, immobilization of nano-sized ZnO onto insoluble supports has become a popular strategy for preparation of high-efficiency photocatalysts.

Graphene currently is receiving considerable attention as a catalyst support in both heterogeneous catalysis and electrocatalysis, due to its high mechanical strength, large surface area, good electrical conductivity, and durability under harsh conditions.[12,13] Some researchers have reported graphene-supported catalysts that exhibit good photocatalytic behaviors for various organic pollutants including methylene blue, methyl orange, Rhodamine B, *p*-chlorophenol, 2,4-dichlorophenoxyacetic acid and Reactive Red 195.[14-17] Enhanced catalytic performance generally is attributed to suppression of photocatalysts' electron-hole recombination. In the process of photocatalysis, graphenes can act as an excellent electron-acceptor/transport material for effective facilitation of the migration of photo-induced electrons and hindrance of charge recombination in electron-transfer processes, which function enhances photocatalytic performance. However, dispersion of catalysts onto graphene entails difficulties due to its hydrophobic nature and tendency to agglomerate. Accordingly, graphene-supported catalysts generally are prepared by first attaching catalysts to the graphene oxide (GO), and then reducing the GO by various chemicals such as hydrazine, dimethylhydrazine, sodium borohydride or strong alkaline solutions. Recently, some researchers have reported that GO-supported catalysts also exhibit better photocatalytic efficiency than pure ZnO particles.[18-23] In this paper, we report a simple and effective process for preparation of GO-supported ZnO (GO-ZnO) using thiolated GO as an efficient photocatalyst for photodegradation of methylene blue (MB).

Experimental

Preparation of Catalysts.

Chemicals: Graphite powder (< 20 μm), potassium persulfate ($K_2S_2O_8$, 99.99%), phosphorus pentoxide (P_2O_5, 99.99%), potassium permanganate ($KMnO_4$, 99%), sodium borohydride ($NaBH_4$, 98%), hydrogen peroxide (H_2O_2, 30%), and zinc acetate dehydrate [$Zn(CH_3COO)_2{\cdot}2H_2O$] were purchased from Sigma-Aldrich. The other reagents were of analytical grade, and were used as received without further purification. All aqueous solutions were prepared with Milli-Q water (> 18.2 MΩ·cm) using a Direct Q3 system (Millipore).

Preparation of Thiolated GO: GO was prepared from graphite powder by the modified Hummers method.[24,25] In brief, the graphite powder (4 g) was first preoxidized with a solution of concentrated H_2SO_4 (60 mL), $K_2S_2O_8$ (2 g), and P_2O_5 (2 g) at 80 °C. The resulting mixture, after cooling to

room temperature, was filtered and washed until the rinse water pH became neutral. The oxidized graphite powder (2 g) was placed in cold (0 °C) concentrated H_2SO_4 (40 mL), and $KMnO_4$ (60 g) was added subsequently under stirring in an ice-bath. The mixture was then stirred at 35 °C for 2 h, after which DI water (92 mL) was added. Next, additional DI water (280 mL) and 30% H_2O_2 solution (50 mL) were added to the mixture to stop the reaction. The resulting mixture was washed by repeated centrifugation and filtration with 5% HCl solution in order to remove the metal ions. Finally, drying under vacuum at 50 °C afforded the GO product. To synthesize thiolated GO, GO (0.5 g) and distilled (DI) water (30 mL) were added to a bottle (250 mL) and ultrasonicated for 20 min. Next, NaSH (8 g) was added gradually with stirring, which mixture was then ultrasonicated for 1 h at 40 °C. Stirring was resumed and maintained for 20 h at 55 °C to produce thiol groups on the GO surfaces. The product finally was filtered and washed with DI water and dried under vacuum for 3 h at 50 °C. The thiolation was confirmed, by reference to the X-ray photoelectron spectroscopy (XPS) spectrum in the sulfur 2p region, to record the characteristic energy at 163 eV.

Preparation of GO-ZnO Catalysts: ZnO nanoparticles were synthesized according to the previously reported sol-gel method.[26] $Zn(CH_3COO)_2{\cdot}2H_2O$ precursor (2.2 g) was dissolved into 100 mL of anhydrous ethanol at 80 °C under vigorous stirring for about 20 min. After the mixture was cooled to 0 °C, $LiOH{\cdot}H_2O$ (0.58 g), dissolved in another 100 mL volume of anhydrous ethanol, was added to the $Zn(CH_3COO)_2{\cdot}2H_2O$ solution under stirring. The mixture was then hydrolyzed for 24 h at 0 °C. Finally, the ZnO alcogels were filtered through a glass-fiber filter for removal of dust and any undissolved $LiOH{\cdot}H_2O$. In the preparation of the GO-ZnO catalysts, thiolated GO sample (0.10 g) was dispersed into 30 mL of anhydrous ethanol under stirring. The prepared ZnO alcogel (30 mL) was added to the GO solution under stirring for 12 h. The GO-ZnO catalyst was then obtained by centrifugation, washed with absolute ethanol, and vacuum dried at 40 °C overnight.

Characterization of Samples. Transmission electron microscopy (TEM) images were obtained with a Tecnai-F20 system operated at 200 kV. Samples for analysis were prepared on a carbon-coated Cu grid by dip-coating in dilute-appropriate solutions (~1.0 wt % solid content). The diameters of 300 decorated nanoparticles were measured using iTEM software (Soft Imaging System GmbH). For non-symmetrical particle shapes, both the largest and shortest distances were measured to obtain an average diameter value. An X-ray diffraction (XRD) analysis was performed using an X'Pert-Pro high-resolution X-ray diffractometer (PANalytical, Netherlands) with Cu Kα radiation (λ = 1.5406 Å). Data were collected at room temperature within the 5-80° range in 0.05° increments. In a surface-chemical analysis, Auger electron spectroscopy (AES) was performed using a PHI 700 scanning Auger nanoprobe with an incident electron energy of 10 keV. The focused-beam diameter was approximately 1.0 μm. XPS measurements were performed on a VG multilab 2000 spectrometer (ThermoVG Scientific) with an unmonochromatized Mg K_α (1253.6 eV) excitation source. Raman spectra were obtained at room temperature using an in *via* Reflex (Renishaw 1000) micro-Raman spectrometer with a 633 nm laser line.

Results and Discussion

Figure 1(a) shows the TEM images of thiolated GO with multi-layered flake-like wrinkled sheets. The GO surface is very smooth. Figures 1(b) and (c) are the GO-ZnO images, which show clearly the presence of a large number of nanoparticles anchored to the sample surface. The adhered nanoparticles in the quasi-spherical morphology are uniformly dispersed on the GO-ZnO surfaces. The corresponding energy-dispersive X-ray (EDX) spectrum of GO-ZnO presents peaks corresponding to the C, O, S, Cu and Zn elements, signaling the existence of ZnO nanoparticles on the GO-ZnO surface [Figure 1(b), inset]. The S element indicates that sulfur-containing groups (mainly thiol groups) were generated in the thiolation. The Cu element is from the basement Cu grid. The corresponding selected-area electron diffraction (SAED) pattern of the GO-ZnO sample shows bright polycrystalline diffraction rings, in agreement with the wurtzite ZnO.[27,28] The adhered precipitates could not be separated from the carbon nanotubes (CNTs), even after thorough washing and prolonged sonication. This particularly strong adhesion might have resulted from the relatively high binding energy (BE) between the ZnO nanoparticles and the thiol groups. Figure 1(d) is a particle-size histogram for GO-ZnO. In order to obtain the particle-size distribution, the histogram was fitted with a Gaussian-shape curve. The ZnO nanoparticles showed an average diameter of 2.5 nm, with a narrow size distribution for GO-ZnO.

The formation of the wurtzite structure in the prepared GO-ZnO sample was further confirmed by XRD. Figure 2

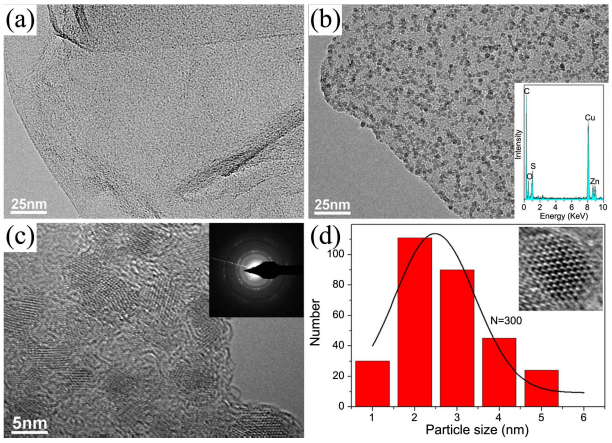

Figure 1. (a) Transmission electron microscopy (TEM) image of thiolated GO. (b) TEM image of GO-ZnO, with corresponding EDX spectrum (inset). (c) HRTEM image of GO-ZnO with corresponding SAED pattern (inset). (d) Size-distribution histograms of ZnO nanoparticles in GO-ZnO, with corresponding atomic-resolved image of the deposited ZnO nanoparticles (inset). The solid line represents the Gaussian fitting curve.

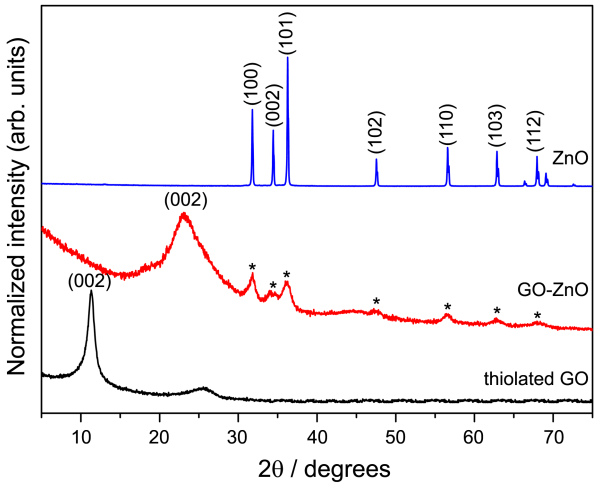

Figure 2. XRD patterns for thiolated GO, GO-ZnO and ZnO, respectively. The peaks marked with an asterisk are those of ZnO in GO-ZnO.

shows the XRD patterns for the thiolated GO, GO-ZnO, and reference ZnO, respectively. The thiolated GO exhibited an intense peak at 11.2° corresponding to the (002) plane interlayer spacing of 0.78 nm, indicating the destruction of the ordinal structures of graphite and the insertion of oxygenous and thiol groups into the interspaces. As for GO-ZnO, distinct diffraction peaks appeared at 2θ = 31.7°, 34.4°, 36.2°, 47.5°, 56.5°, 62.8°, and 67.9°, corresponding respectively to the (100), (002), (101), (102), (110), (103), and (112) crystalline planes of hexagonal wurtzite ZnO (JCPDS No. 36-1451). These observations confirmed that the wurtzite ZnO nanoparticles were effectively anchored to the GO surface.

After nanoparticle deposition, there is a significant shifting and broadening on the (002) plane of thiolated GO toward a higher 2θ value. Although the reason, thus far, remains unclear, both shifting and broadening are occasionally observed in functionalized or decorated GO.[29,30] This might be due to disruption in the initial layered organization of GO, which resulted in an increased interlayer distance between the sheets.

Figure 3(a) plots the Auger spectroscopic data for GO-ZnO. The S, C, O, and Zn peaks were detected in the spectra at 155, 275, 520, and 996 eV, respectively. The Zn content within the samples was estimated from the Auger peak areas and corrected according to the tabulated sensitivity factors. The estimated value of the Zn content was nearly 7.3% for Go-ZnO. The oxidation state of the Zn species anchored to the GOs was verified by XPS. Figure 3(b) shows the Zn 2p XPS spectra for GO-ZnO. The Zn 2p spectrum consists of two peaks including Zn $2p_{3/2}$ and Zn $2p_{1/2}$, which correspond to 1022 and 1045 eV. These BE values are in good agreement with those reported for hexagonal wurtzite ZnO.[31]

Figure 4 provides the Raman spectra of the thiolated GO and GO-ZnO. That of thiolated GO exhibited two intense peaks at 1337 and 1597 cm^{-1}, corresponding to the D and G bands, respectively. The intensity of the D band (the

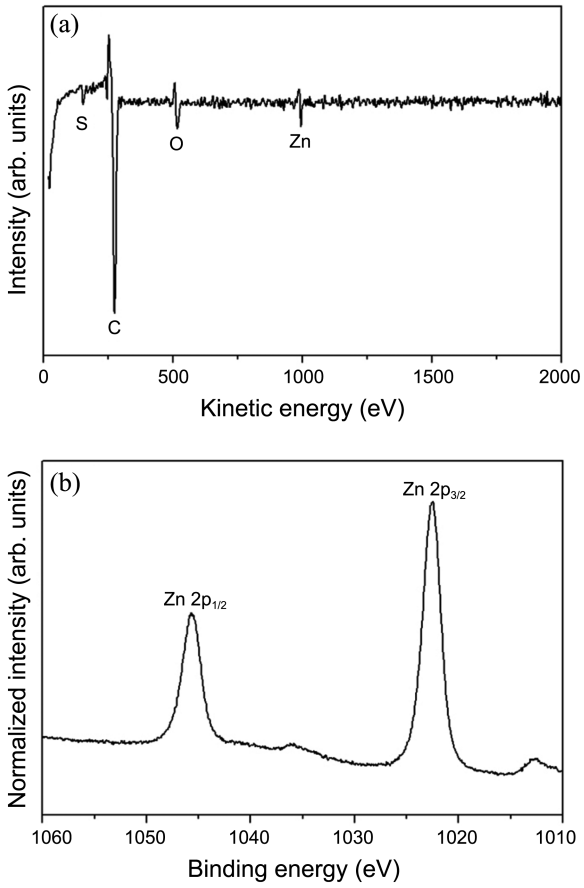

Figure 3. (a) Auger spectrum for GO-ZnO. (b) Zn 2p core-level spectra for GO-ZnO.

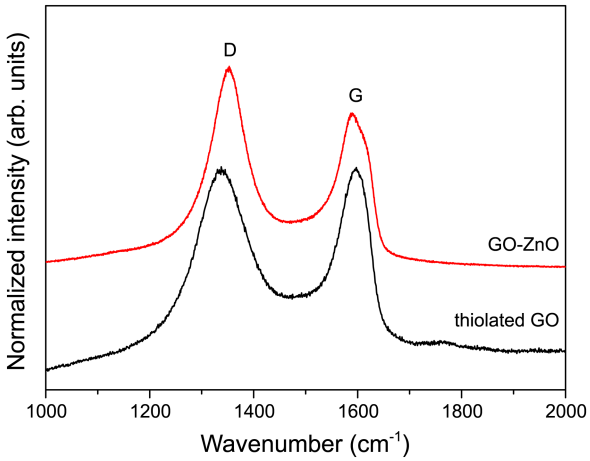

Figure 4. Raman spectra for thiolated GO and GO-ZnO.

symmetrical A_{1g} mode) reflects the degree of edge chirality, and the G band (the E_{2g} mode of sp^2 carbon atoms), the relative degree of graphitization.[32] The D/G band intensity ratio (I_D/I_G) is in linear relation to the inverse of the in-plane crystallite dimension. The I_D/I_G value is about 1.02 for the thiolated GOs, and about 1.30 for the GO-ZnO. These results suggest that the deposition of ZnO onto thiolated GOs results in a decrease of their crystallinity due to the perturbation of GO's initial layered organization, which is in agreement

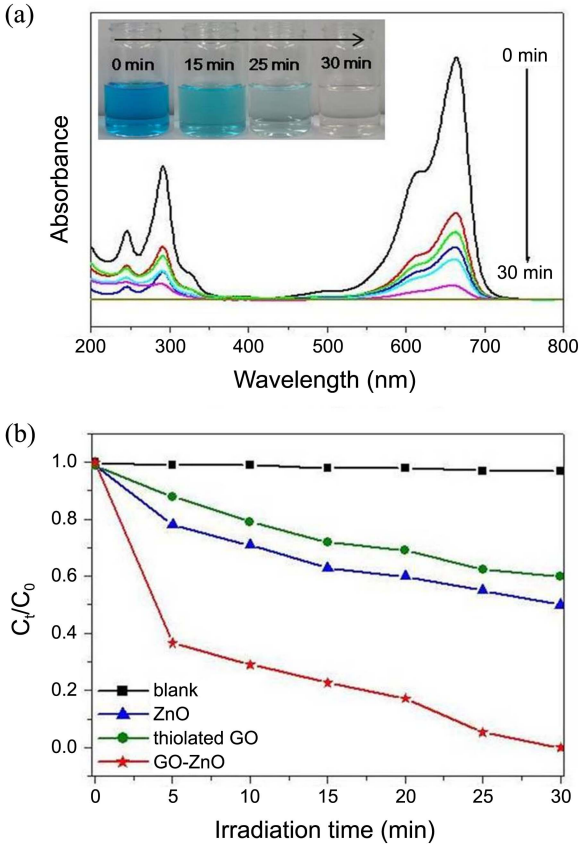

Figure 5. (a) UV-visible spectra of MB solution (2.0 mM) in presence of ZnO-GO catalyst and UV irradiation, with corresponding MB solution color-change sequence (inset). (b) Photocatalytic activity of ZnO, thiolated GO, and GO-ZnO degradation of MB under UV irradiation. C_0 is the initial concentration of MB, and C_t is the MB concentration at reaction time t.

with the XRD results.

The MB-degrading photocatalytic activities of the prepared GO-ZnO catalysts were evaluated under UV irradiation. Figure 5(a) plots the change in the absorption spectra of MB as a function of irradiation time in the presence of GO-ZnO. It can be seen that the maximum absorbance at 665 nm rapidly decreases with the increase in irradiation time and disappears almost completely after 30 min. The lack of any new-appearing peak in the course of the reaction signaled that degradation had been successfully completed. To elucidate the synergy-induced enhancement of GO-ZnO's photocatalytic efficiency, comparative experiments were performed using ZnO nanoparticles, thiolated GO, and GO-ZnO in the photodegradation of MB, respectively. The results of the MB degradation with respect to light-exposure durations ranging from 0 to 30 min are shown in Figure 5(b). The "blank" experiment, without any photocatalyst, showed that no activity had occurred under UV irradiation. By contrast, when the catalyst is added to the solution, noticeable MB degradation occurred. The degradation of MB was about 40, 50 and 100% for the thiolated GO, pristine ZnO, and GO-ZnO, respectively, indicating that the efficiency of the pristine ZnO catalysts was greatly enhanced by deposition on the thiolated GO surfaces. Such enhanced photocatalytic performance can be attributed to the excellent electronic conductivity and enhanced mass transportation, which facilitates photo-induced electron transport to the surface of the catalysts, thereby inhibiting recombination of photo-induced electrons and holes.[21,33,34] Adsorption of organic molecules also is favored by π-π interaction between thiolated GOs and aromatic rings, thus leading to favorable reactant-product mass transportation.

Conclusions

We demonstrated that thiolated GO can be effectively used as a photocatalyst support for MB-degradation purposes. TEM observations revealed that well-dispersed ZnO nanoparticles were anchored to the surfaces of the thiolated GOs and that the average particle diameter was about 2.5 nm. The SEAD and XRD results indicated, moreover, that the wurtzite ZnO nanoparticles had effectively anchored to the GO surface. The estimated ZnO content in the GO-ZnO was nearly 7.3%. As for the photodegradation of MB under UV light, GO-ZnO exhibited a much higher photocatalytic efficiency than the thiolated GOs or pristine ZnO particles. This enhanced photocatalytic performance of GO-ZnO can be attributed to the suppression of electron recombination and the enhancement of mass transportation. The results further suggest that the GOs had significantly influenced the photocatalytic activities of the GO-supported catalysts' organic-pollutant degradation.

Acknowledgments. This research was supported by the Basic Science Research Program through the National research Foundation of Korea (NRF) funded by the Ministry of Education, Science and Technology (2010-0003963). Authors thank for TEM analysis from the Korea Basic Science Institute (KBSI) - Gwangju branch in Chonnam National University.

References

1. Zhang, W.-D.; Xu, B.; Jiang, L.-C. *J. Mater. Chem.* **2010**, *20*, 6383-6391.
2. Puma, G. L.; Bono, A.; Krishnaiah, D.; Collin, J. G. *J. Hazard. Mater.* **2008**, *157*, 209-219.
3. Akyol, A.; Bayramoglu, M. *J. Hazard. Mater.* **2010**, *175*, 484-491.
4. Khan, S. B.; Faisal, M.; Rahman, M. M.; Jamal, A. *Talanta* **2011**, *85*, 943-949.
5. Li, J.; Lu, G.; Wang, Y.; Guo, Y.; Guo, Y. *J. Colloid Interface Sci.* **2012**, *377*, 191-196.
6. Yassitepe, E.; Yatmaz, H. C.; Öztürk, C.; Öztürk, K.; Duran, C. *J. Photochem. Photobiol. A-Chem.* **2008**, *198*, 1-6.
7. Lv, T.; Pan, L.; Liu, X.; Lu, T.; Zhu, G.; Sun, Z. *J. Alloy. Compd.* **2011**, *509*, 10086-10091.
8. Wang, H.; Xie, C.; Zhang, W.; Cai, S.; Yang, Z.; Gui, Y. *J. Hazard. Mater.* **2007**, *141*, 645-652.
9. Xiang, Q.; Meng, G.; Zhang, Y.; Xu, J.; Xu, P.; Pan, Q.; Yu, W. *Sens. Actuator B-Chem.* **2010**, *143*, 635-640.
10. Xia, J.; Wang, A.; Liu, X.; Su, Z. *Appl. Surf. Sci.* **2011**, *257*, 9724-9732.
11. Ba-Abbad, M. M.; Kadhum, A. A. H.; Mohamad, A. B.; Takriff,

M. S.; Sopian, K. *J. Alloy. Compd.* **2013**, *550*, 63-70.
12. Antolini, E. *Appl. Catal. B-Environ.* **2012**, *123-124*, 52-68.
13. Wu, G.; Wang, X.; Guan, N.; Li, L. *Appl. Catal. B-Environ.* **2013**, *136-137*, 177-185.
14. Ismail, A. A.; Geioushy, R. A.; Bouzid, H.; Al-Sayari, S. A.; Al-Hajry, A.; Bahnemann, D. W. *Appl. Catal. B-Environ.* **2013**, *129*, 62-70.
15. Wang, J.; Wang, P.; Cao, Y.; Chen, J.; Li, W.; Shao, Y.; Zheng, Y.; Li, D. *Appl. Catal. B-Environ.* **2013**, *136-137*, 94-102.
16. Hou, Y.; Li, X.; Zhao, Q.; Chen, G. *Appl. Catal. B-Environ.* **2013**, *142-143*, 80-88.
17. Ghasemi, S.; Esfandiar, A.; Setayesh, S. R.; Habibi-Yangjeh, A.; Iraji zad, A.; Gholami, M. R. *Appl. Catal. A-Gen.* **2013**, *462-463*, 82-90.
18. Fu, D.; Han, G.; Chang, Y.; Dong, J. *Mater. Chem. Phys.* **2012**, *132*, 673-681.
19. Li, B.; Liu, T.; Wang, Y.; Wang, Z. *J. Colloid Interface Sci.* **2012**, *377*, 114-121.
20. Ameen, S.; Akhtar, M. S.; Seo, H.-K.; Shin, H. S. *Mater. Lett.* **2013**, *100*, 261-265.
21. Chen, Y.-L.; Zhang, C.-E.; Deng, C.; Fei, P.; Zhong, M.; Su, B.-T. *Chin. Chem. Lett.* **2013**, *24*, 518-520.
22. Sun, L.; Shao, R.; Tang, L.; Chen, Z. *J. Alloys Compd.* **2013**, *564*, 55-62.
23. Kumar, S. V.; Huang, N. M.; Yusoff, N.; Lim, H. N. *Mater. Lett.* **2013**, *93*, 411-414.
24. Kovtyukhova, N. I.; Olliver, P. J.; Martin, B. R.; Mallouk, T. E.; Chizhik, S. A.; Buzaneva, E. V.; Gorchinskiy, A. D. *Chem. Mater.* **1999**, *11*, 771-778.
25. Kim, J. D.; Palani, T.; Kumar, M. R.; Lee, S.; Choi, H. C. *J. Mater. Chem.* **2012**, *22*, 20665-20670.
26. Singh, G.; Choudhary, A.; Haranath, D.; Joshi, A. G.; Singh, N.; Singh, S.; Pasricha, R. *Carbon* **2012**, *50*, 385-394.
27. Maensiri, S.; Masingboon, C.; Promarak, V.; Seraphin, S. *Opt. Mater.* **2007**, *29*, 1700-1705.
28. He, C.; Sasaki, T.; Shimizu, Y.; Koshizaki, N. *Appl. Surf. Sci.* **2008**, *254*, 2196-2202.
29. Pham, V. H.; Cuong, T. V.; Hur, S. H.; Oh, E.; Kim, E. J.; Shin, E. W.; Chung, J. S. *J. Mater. Chem.* **2011**, *21*, 3371-3377.
30. Orth, E. S.; Fonsaca, J. E. S.; Domingues, S. H.; Mehl, H.; Oliveira, M. M.; Zarbin, A. J. G. *Carbon* **2013**, *61*, 543-550.
31. Shan, G.; Zhong, M.; Wang, S.; Li, Y.; Liu, Y. *J. Colloid Interface Sci.* **2008**, *326*, 392-395.
32. Liu, Z.; Xu, W.; Fang, J.; Xu, X.; Wu, S.; Zhu, X.; Chen, Z. *Appl. Surf. Sci.* **2012**, *259*, 441-447.
33. Zhang, L.; Du, L.; Cai, X.; Yu, X.; Zhang, D.; Liang, L.; Yang, P.; Xing, X.; Mai, W.; Tan, S.; Gu, Y.; Song, J. *Physica E* **2013**, *47*, 279-284.
34. Xu, T.; Zhang, L.; Cheng, H.; Zhu, Y. *Appl. Catal. B-Environ.* **2011**, *101*, 382-387.